Electronic Supplementary Information: Generation and Study of Am(IV) by Temperature-Dependent Electron Pulse Radiolysis

Amy E. Kynman,[ab*] Travis S. Grimes,[a] Stephen P. Mezyk,[c] Bobby Layne,[d] Andrew R. Cook,[d] Brian M. Rotermund,[e] and Gregory P. Horne[a*]

[a] *Center for Radiation Chemistry Research, Idaho National Laboratory, 1955 N. Freemont Ave., Idaho Falls, ID, 83415, USA.*

[b] *Glenn T. Seaborg Institute, Idaho National Laboratory, Idaho Falls, ID, 83415, USA.*

[c] *Department of Chemistry and Biochemistry, California State University Long Beach, 1250 Bellflower Blvd., Long Beach, CA 90840, United States*

[d] *Department of Chemistry, Brookhaven National Laboratory, Upton, New York, 11973, USA*

[e] *Department of Chemistry, Colorado School of Mines, Golden, Colorado 80401, USA*

*Corresponding authors. E-mail: amy.kynman@inl.gov and gregory.holmbeck@inl.gov

Methodology

Caution! The americium solutions employed in this work were highly radioactive. Handling was performed in dedicated radiological and nuclear facilities using well-established radiological safety protocols.

Materials

Americium was acquired as americium oxide (99.9% $^{243}Am_2O_3$, 0.1% $^{241}Am_2O_3$) from on-hand stock at Idaho National Laboratory (INL). Deionized water (DI H_2O, ultra-pure HPLC grade), hydrochloric acid (HCl, 37 wt.%), nitric acid (HNO_3, ≥99.999% trace metals basis), perchloric acid ($HClO_4$, ≥99.999% trace metals basis), sodium persulfate ($Na_2S_2O_8$, , 99.99% trace metal basis) and ethylenediaminetetraacetic acid (EDTA, purified grade) were purchased from MilliporeSigma (Burlington, MA, USA). Unless otherwise stated, all chemicals were used without further purification.

Sample Preparation

An americium (Am) stock solution was first purified via column chromatography using a 10 mL column with 2 mL DGA resin. Am loaded solution (100 mL) was acidified to 4.0 M HNO_3 with concentrated HNO_3 and passed through the column at a rate of 0.5 mL min^{-1}, forming a pink band of Am(III) at the top of the column. After the loaded solution was eluted, the column was rinsed with 15 mL of 6.0 M HNO_3 to ensure removal of all organic impurities present. The column was then rinsed with 6 mL of 8.0 M HCl. After the initial HCl rinse, the Am was subsequently eluted with 20 mL of 0.02 M HCl. The pink Am(III) band migrated down the column after 1–2 mL of the eluent was passed, and was completely eluted following 10 mL of eluent. The remaining 10 mL of eluent was passed to ensure all Am was recovered.

The aforementioned purification procedure was then repeated on a second Am stock solution. The resulting solutions were combined to give 20 mL of 0.02 M HCl containing approximately 6 mg of Am(III), which was divided into two solutions containing approximately 3 mg of Am(III) each. Metathesis reactions were then performed on each Am(III) solution. The metathesis apparatus, consisting of a three-necked round bottom flask positioned in a heated sand bath, addition funnel, distillation bridge, and three-necked receiving flask is shown below in **Fig. S1**. The apparatus was held under a flow of air while being heated, and the receiving flask connected to an EDTA scrub solution.

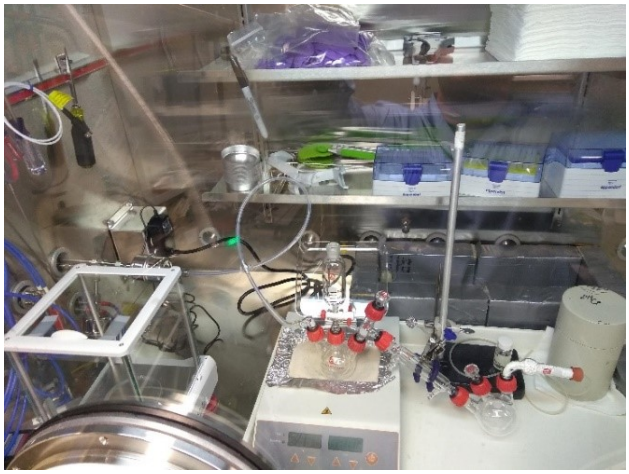

Fig. S1. Experimental set-up for Am(III) metathesis.

The first metathesis was performed to change the background electrolyte from HCl to HNO_3. The initial Am(III)/HCl solution was introduced to the round bottom flask and heated to evaporate the HCl until a green residue remained. The residue was then dissolved in 2 mL of DI H_2O and evaporated back to residue with gentle heating. The evaporation cycles were repeated six times following which the remaining residue was pink in color, indicating that HCl had been completely removed. The residue was then

redissolved in 5 mL of 6.0 M HNO_3. The same exact procedure was followed for the conversion of the second Am(III)/HCl solution to $HClO_4$, with the pink residue instead being dissolved in 0.100 M $HClO_4$, resulting in two Am(III) stock solutions which were standardized by UV-Visible spectroscopy (UV-Vis) using Am(III) extinction coefficients reported in the literature.[1]

Each of the purified americium stock solutions were then used to prepare two sample series, the formulation of each designed to promote the formation of a given radical species. For the nitrate radical ($NO_3^{\bullet}$), the Am/HNO_3 stock was diluted with 6.0 M HNO_3 to give samples with americium concentrations of approximately 0.5, 0.75, 1, or 2 mM in 6.0 M HNO_3 as determined by UV-Vis spectroscopy.

For the sulfate radical anion ($SO_4^{\bullet-}$) the Am/$HClO_4$ stock solution was initially diluted by a factor of 1.58 with a solution of 0.1 M $Na_2S_2O_8$ in 0.10 M $HClO_4$. Subsequent dilutions were performed using a 0.1 M $Na_2S_2O_8$/0.0634 M $HClO_4$ solution to produce four samples with concentrations of approximately 0.50, 0.75, 1.0, and 2.0 mM with respect to Am(III), 0.100 M with respect to $Na_2S_2O_8$, and 0.0634 M with respect to $HClO_4$. All Am(III) sample solutions were transferred to 1.0 cm optical pathlength, screwcap sealed, spectrosil quartz, semi-micro, Suprasil Starna Scientific Ltd. (Ilford, United Kingdom) cuvettes for irradiation.

Note: A portion of the Am/HNO_3 stock solution was oxidized with excess sodium bismuthate (45 mg/mL) and diluted with the intention of preparing samples containing hexavalent americium (approximately 0.5, 0.75, 1, 2 mM) for pulse radiolysis studies. At the time of sample measurement, UV-Vis spectroscopy indicated complete reduction of Am(VI) to primarily Am(III) with some percentage of Am(V) (**Fig. S4**). The highest concentration sample in this series was therefore used as a duplicate sample for studying the reaction of Am(III) with $NO_3^{\bullet}$, following deconvolution of Am(III) and Am(V) using the published rate constant (k = 2.5 × 10^8 M^{-1} s^{-1})[2] for the reaction between Am(V) and $NO_3^{\bullet}$. This value is used in **Fig. S10B** and the subsequent rate coefficient determination for the reaction between Am(III) and $NO_3^{\bullet}$ at 21.9 ± 0.5 °C.

Pre- and Post-irradiation Sample Absorption Spectra

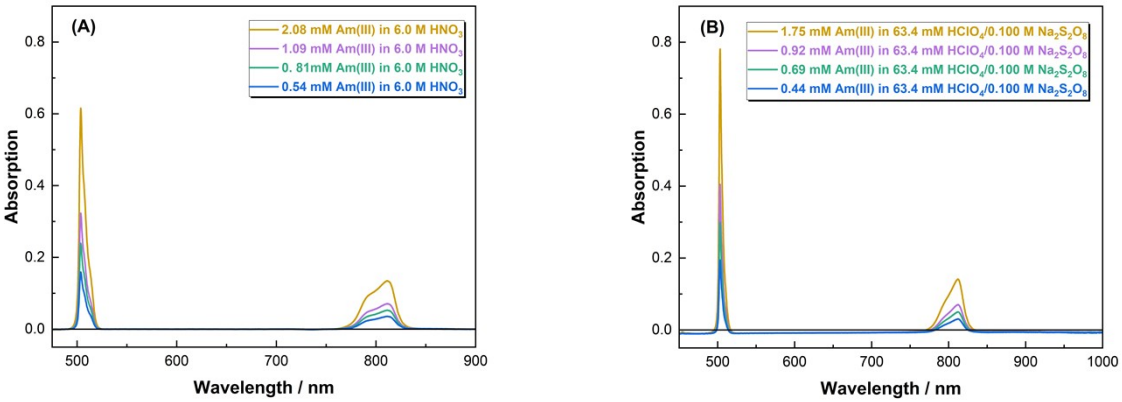

Fig. S2. Absorption spectra of HNO_3 **(A)** and $HClO_4$ **(B)** samples containing Am(III) measured prior to irradiation.

Prior to irradiation the Am(III) content in each sample was quantified in triplicate by UV-Vis spectroscopy (**Fig. S2**). The molar extinction coefficient for the 503 nm peak corresponding to Am(III) has been well documented in the literature at a range of acid and americium concentrations. A value of $\varepsilon(503) = 296$ M^{-1} cm^{-1} was used for Am(III) samples in 6 M HNO_3, and a value $\varepsilon(503) = 448$ M^{-1} cm^{-1} for Am(III) samples in dilute $HClO_4$, as reported by Zalupski *et al*.[1]

Following irradiation, the Am(III) concentration of the highest concentration Am(III)/HNO_3 sample (ca. 2.08 mM) was redetermined by UV-Vis spectroscopy to ensure no appreciable loss of Am(III) (**Fig. S3**). No change in Am(III) concentration in the sample before and after irradiation was observed.

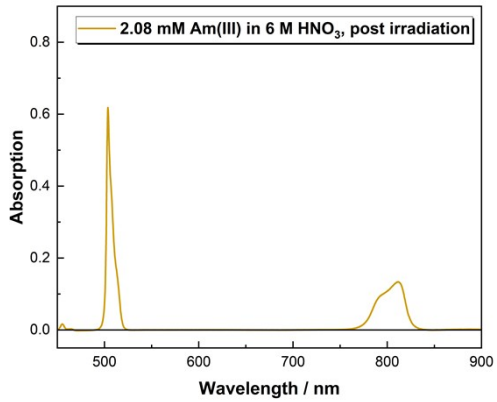

Fig. S3. Absorption spectra of the 2.08 mM Am(III)/HNO_3 sample measured post irradiation.

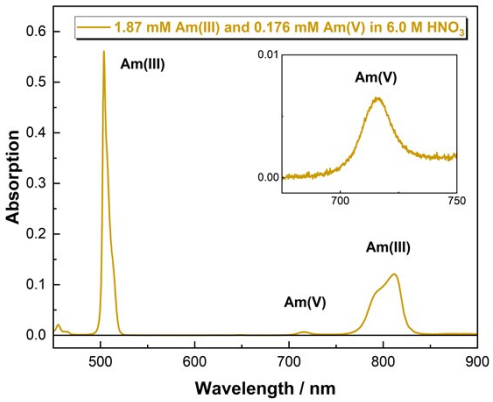

Fig. S4. Absorption spectra of the 2.05 mM Am/HNO_3 sample following oxidation with sodium bismuthate.

Time-resolved Electron Pulse Irradiations

Chemical kinetics and activation parameters were determined for the reaction of Am(III) with $NO_3^{\bullet}$ and $SO_4^{\bullet-}$ using the Brookhaven National Laboratory Laser Electron Accelerator Facility; the detection system for this capability has been previously described.[3] Acquisition of temperature dependent measurements involved the use of a custom-built, temperature-controlled cuvette holder, shown in **Fig. S5**.

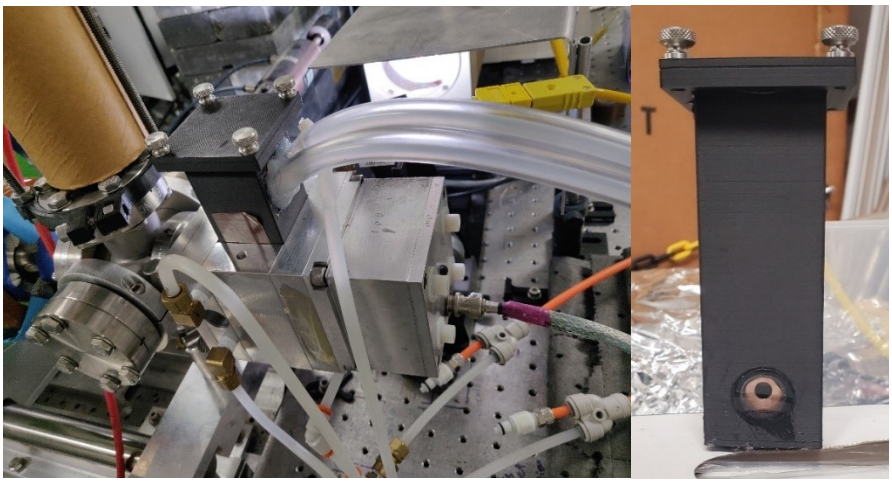

Fig. S5. Temperature-controlled cuvette holder designed for the analysis of radiation-induced actinide chemical kinetics as a function of temperature.

This brand-new capability consists of a brass cell block, containing space for a K-type thermocouple, through which water from a heat exchanger flows. The cell holder is surrounded by 3D printed secondary containment, constructed of nylon chopped carbon fiber, measuring 1.5 × 1.5 × 4.5 inches. The secondary containment vessel contains a thumb screw-secured lid, and a 19 mm diameter × 1 mm thick S1 grade quartz window, behind which sits a copper plate with a 0.25 inch diameter hole to clip the analysing light

path. Tygon tubing water lines, leading inside and outside of the sample holder, were sealed with epoxy resin to completely encapsulate the sample. The temperature inside the sealed cuvette holder was controlled by a standard chiller bath/heater (NesLab RTE-111). Temperature variations were determined to be less than ± 1 °C during each experiment, for which measurements were taken over the course of 5–10 minutes.

Once loaded in the new sample holder, the americium samples were irradiated with 9 MeV electron pulses, averaging four pulses for improved signal to noise. Dosimetry was determined using a water solution containing 20% methanol and 1 M NaOH,[4, 5] affording an average dose of 18 Gy per pulse. For kinetic measurements, each sample was exposed to four pulses per experiment in triplicate, while the measurement of transient absorption spectra involved three electron pulses per experiment per wavelength.

Kinetic measurements were performed at 8.8, 21.9, 30.3, and 40.1 ± 0.5 °C, and monitored up to 17 µs after the electron pulse. For $NO_3^{\bullet}$, chemical kinetics were measured at 365 nm (growth and decay of Am(IV)) and 632 nm (decay of $NO_3^{\bullet}$). For $SO_4^{\bullet-}$, chemical kinetics were measured at 365 nm (growth and decay of Am(IV)) and 450 nm (decay of $SO_4^{\bullet-}$).

Chemical kinetics were derived by fitting the decay of both radicals with a double exponential decay function:

$$Abs = \mathrm{Abs_x} * e^{(-kxt)} + \mathrm{Abs_y} * e^{(-kyt)} + B, \quad (1)$$

where *Abs* is the measured time-dependent absorbance of the radical, Abs_x and Abs_x are fitted absorbances, and *B* allows for any limiting product absorption (baseline shift). The faster k_X rate coefficient corresponds to short timescale processes involving other radiolysis products, such as the hydroxyl radical ($^{\bullet}$OH). The slower k_Y rate coefficient corresponds to various longer timescale processes, including reactions with water molecules and other solutes, as demonstrated for the decay mechanism of $NO_3^{\bullet}$ in nitrate and HNO_3 media.[6]

The growth and decay of the Am(IV) signal at 365 nm was fit with a sequential, exponential growth and decay function:

$$Abs = \frac{Abs^{o} * k_1}{(k_2 - k_1)} * \left(e^{-k_1 t} - e^{-k_2 t}\right) + B, \quad (2)$$

where *Abs* is the measured time-dependent absorbance of the transient, Abs^o is the fitted initial absorbance, k_X is the pseudo-first-order growth of the transient, corresponding to the reaction of the radical (ca. 5 μM) with the Am(III) (ca. 400–2000 μM) present:

$$NO_3^{\bullet}/SO_4^{\bullet-} + \text{Am(III)} \rightarrow NO_3^{-}/SO_4^{2-} + \text{Am(IV)} \qquad k_{x,} \qquad (3)$$

k_y is the fitted first-order decay of the Am(IV) transient:

$$\text{Am(IV)} \rightarrow \text{products} \qquad k_{y,} \qquad (4)$$

and *B* is a baseline adjustment parameter.

Arrhenius parameters (activation energy, E_a, and pre-exponential factor, *A*) were derived from the following linear equation:

$$ln(k) = -\frac{Ea}{RT} + ln(A), \qquad (5)$$

where *k* is the second-order rate coefficient (M^{-1} s^{-1}) derived from **Eq. 1** and **2**, *R* is the Ideal Gas Constant (8.314 J mol K^{-1}), and *T* is the absolute temperature (K).

Eyring activation parameters (enthalpy of activation, $\Delta H^{\dagger}$, and entropy of activation, $\Delta S^{\ddagger}$) were derived from the following linear equation:

$$ln\left(\frac{k}{T}\right) = -\frac{\Delta H \dagger}{RT} + ln\frac{kB}{h} + \frac{\Delta S \ddagger}{R}, \qquad (6)$$

where k_B is Boltzmann's constant (1.381 × 10-23 J K^{-1}), *h* is Plank's constant (6.626 × 10^{-34} J s), and *k*, *R*, and T are, again, the second-order rate coefficient, Ideal Gas Constant, and absolute temperature, respectively.

As $SO_4^{\bullet-}$ is negatively charged and Am(III) is positively charged, the derived second-order rate coefficients were corrected for the ionic strength of each sample solution to account for the effects of coulombic attraction using **Eq. 8**:[7]

$$\log(k_0) = \log(k) - 2Z_{\alpha}Z_{\beta}\left(\frac{A\mu^{\frac{1}{2}}}{1 + \mu^{\frac{1}{2}}}\right), \qquad (7)$$

where k_0 is the rate coefficient (M^{-1} s^{-1}) at zero ionic strength, k is the rate coefficient measured here at a total ionic strength μ (mol L^{-1}), Z_α and Z_β are the respective charges of the radical anions (Z_α = −1), and Am(III) (Z_β = +3), respectively, and A is the temperature-dependent Debye–Hückel constant, **Eq. 8**:[8]

$$A = \frac{e^3(2000 \times N_A)^{\frac{1}{2}}}{2.303(8\pi)(\varepsilon_0 \varepsilon k_B T)^{\frac{3}{2}}}, \quad (8)$$

where e is the charge of an electron (1.602×10^{-19} C), N_A is Avogadro's number (6.022×10^{23} mol^{-1}), ε_0 is the vacuum permittivity (8.854×10^{-12} F m^{-1}), ε is the dielectric constant for water (78.84), and k_B is the Boltzmann constant (1.380×10^{-23} J K^{-1}).

Quoted errors (1s) are a quantitative combination of measurement precision (~2–4%) and sample concentration (initial concentration (5–9%) and dilution (< 1%)) errors.

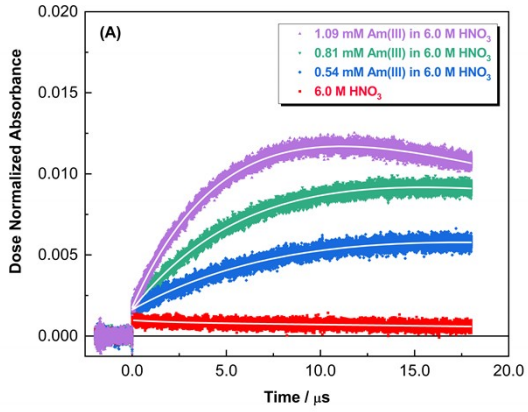

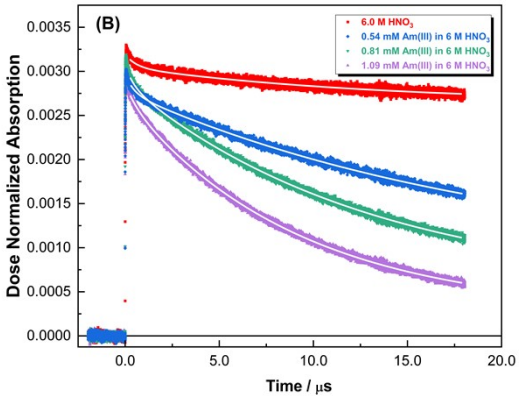

Am(III) + $NO_3^\bullet$ Chemical Kinetics

Fig. S6. Growth and decay kinetics of Am(IV) at 365 nm **(A)** and $NO_3^{\bullet}$ at 632 nm **(B)** at 8.8 °C.

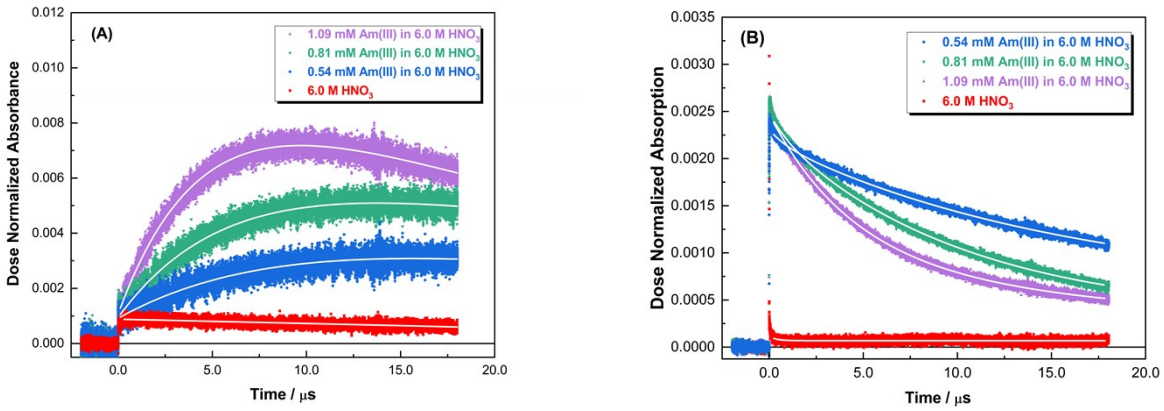

Fig. S7. Growth and decay kinetics of Am(IV) at 365 nm **(A)** and $NO_3^{\bullet}$ at 632 nm **(B)** at 30.3 °C.

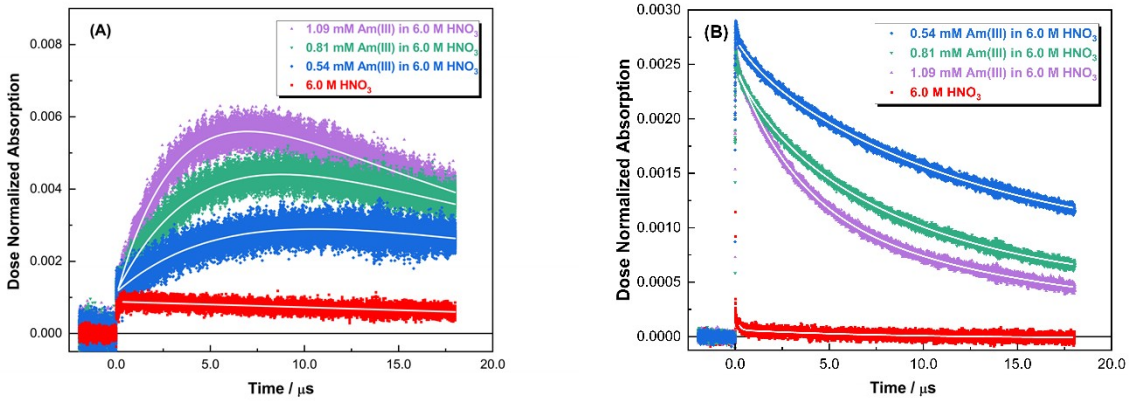

Fig. S8. Growth and decay kinetics of Am(IV) at 365 nm **(A)** and $NO_3^{\bullet}$ at 632 nm **(B)** at 40.1 °C.

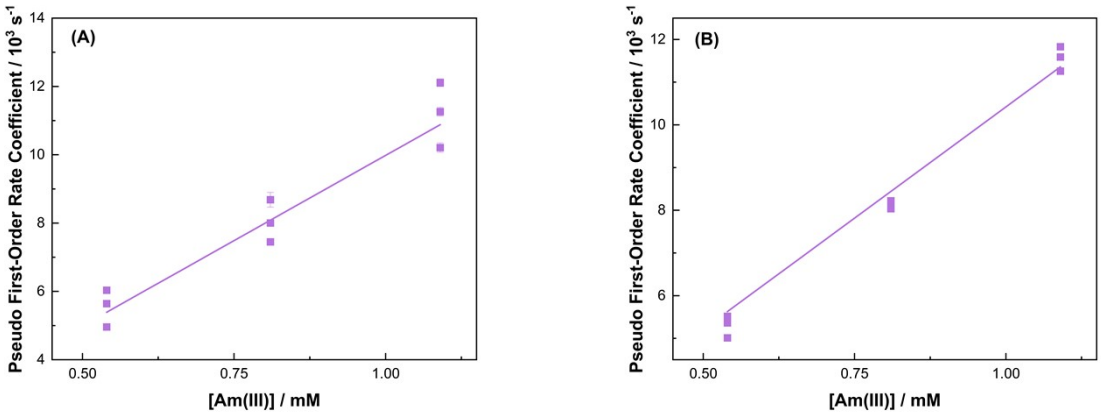

Fig. S9. Second-order rate coefficient determination by plotting derived first-order component values of **(A)** the growth of Am(IV) and **(B)** the decay of the $NO_3^{\bullet}$ radical measured at 8.8 °C against Am(III) concentration. This afforded values of $k_{8.8\,°C}$(Am(III) + $NO_3^{\bullet}$) = (9.98 ± 0.85) × 10^7 M^{-1} s^{-1}, R^2 = 0.99 **(A)** and (1.04 ± 0.01) × 10^8 M^{-1} s^{-1}, R^2 = 0.99 **(B)**. Note that some error bars are smaller than the presented data points.

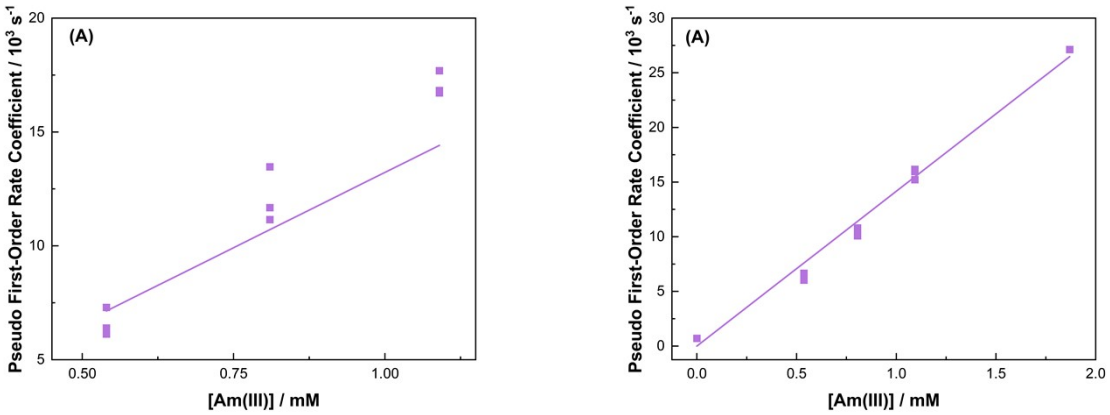

Fig. S10. Second-order rate coefficient determination by plotting derived first-order component values of **(A)** the growth of Am(IV) and **(B)** the decay of the $NO_3^{\bullet}$ radical measured at 21.9 °C against Am(III) concentration. This afforded values of $k_{21.9\,°C}$(Am(III) + $NO_3^{\bullet}$) = (1.32 ± 0.06) × 10^8 M^{-1} s^{-1}, R^2 = 0.98 **(A)** and (1.38 ± 0.03) × 10^8 M^{-1} s^{-1}, R^2 = 0.99 **(B)**. Note that some error bars are smaller than the presented data points.

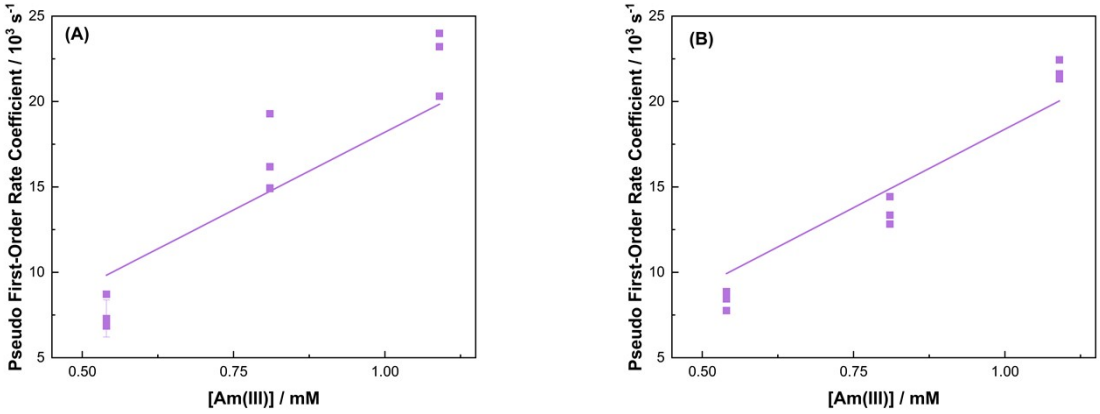

Fig. S11. Second-order rate coefficient determination by plotting derived first-order component values of **(A)** the growth of Am(IV) and **(B)** the decay of the $NO_3^{\bullet}$ radical measured at 30.3 °C against Am(III) concentration. This afforded a value of $k_{30.3°C}$(Am(III) + $NO_3^{\bullet}$) = (1.82 ± 0.12) × 10^8 M^{-1} s^{-1}, R^2 = 0.96 **(A)** and (1.84 ± 0.07) × 10^8 M^{-1} s^{-1}, R^2 = 0.99 **(B)**. Note that some error bars are smaller than the presented data points.

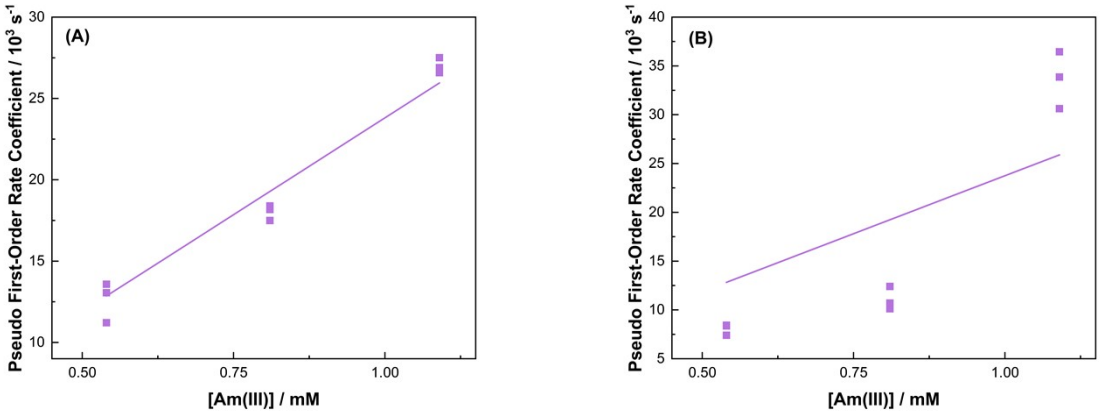

Fig. S12. Second-order rate coefficient determination by plotting derived first-order component values of **(A)** the growth of Am(IV) and **(B)** the decay of the $NO_3^{\bullet}$ radical measured at 40.1 °C against Am(III) concentration. This afforded a value of $k_{40.1°C}$(Am(III) + $NO_3^{\bullet}$) = (2.38 ± 0.05) × 10^8 M^{-1} s^{-1}, R^2 = 0.99 **(A)** and (2.37 ± 0.30) × 10^8 M^{-1} s^{-1}, R^2 = 0.87 **(B)** respectively. Note that some error bars are smaller than the presented data points.

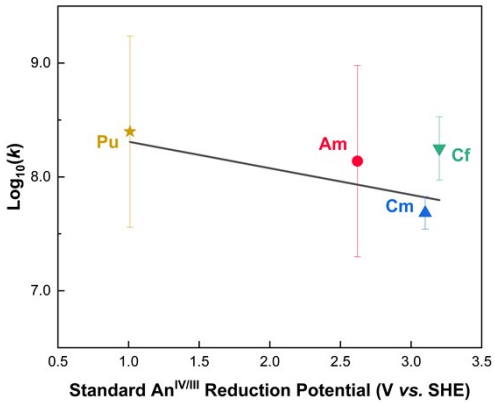

Fig. S13. Second-order rate coefficients for the reaction of $NO_3^{\bullet}$ with trivalent actinide ions[9-12] plotted against the standard reduction potentials for their IV/III couples.[13]

Am(III) + $SO_4^{\bullet-}$ Transient Absorption Spectra

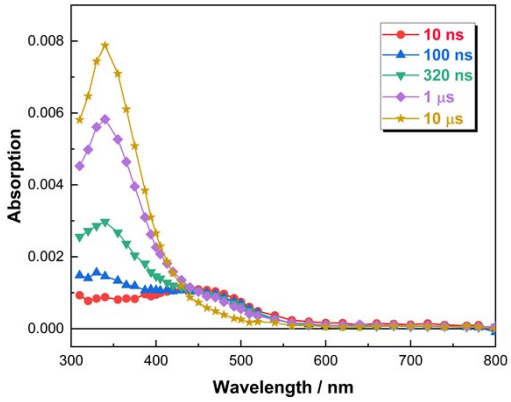

Fig. S14. Dose normalized transient absorption spectra from the electron pulse irradiation of 1.75 mM Am(III) in aerated 6.0 M HNO_3 at 21 ± 1 °C for several time slices after the electron pulse.

Am(III) + $SO_4^{\bullet-}$ Chemical Kinetics

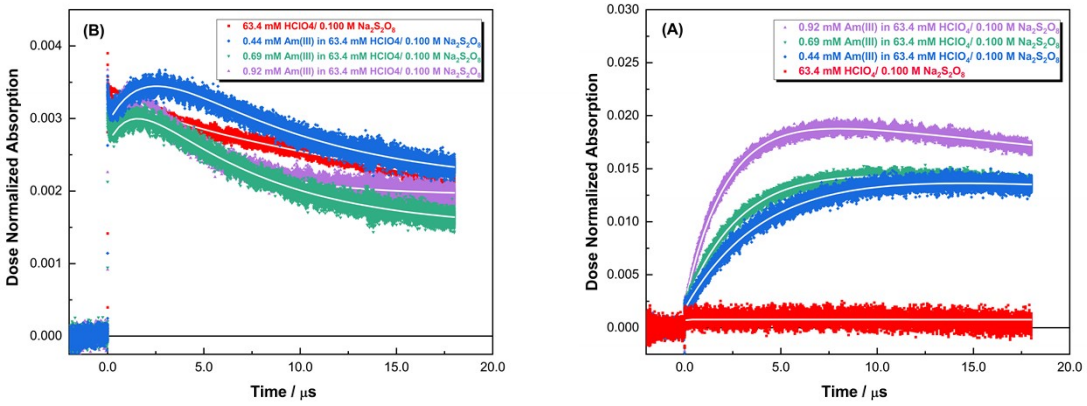

Fig. S15. Growth and decay kinetics of Am (IV) at 365 nm **(A)** and $SO_4^{\bullet}$ at 450 nm **(B)** at 21.9 °C.

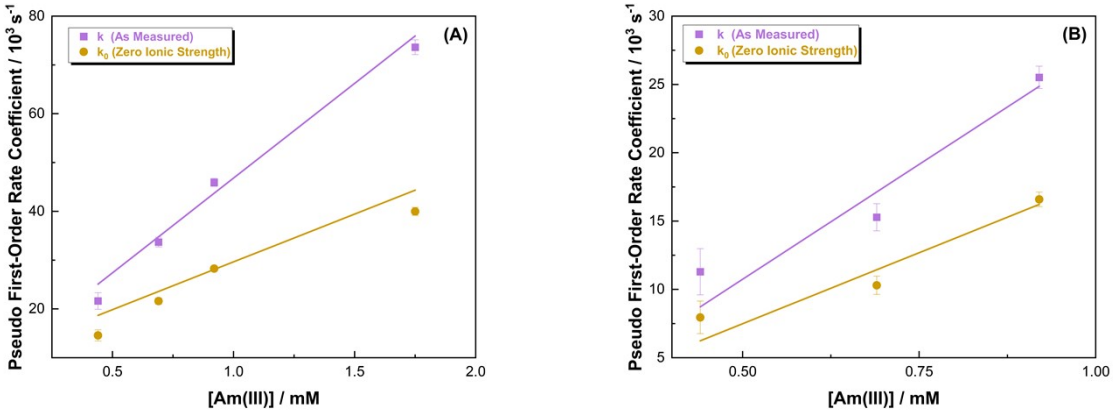

Fig. S16. Second-order rate coefficients determined by plotting derived first-order component values for the growth of Am(IV) **(A)** and the decay of $SO_4^{\bullet-}$ **(B)** against solute concentration with (**gold ●**) and without (**purple ■**) ionic strength corrections. This afforded an ionic strength-corrected value of k(Am(III) + $SO_4^{\bullet-}$) = (1.96 ± 0.32) × 10^8 M^{-1} s^{-1}, R^2 = 0.92 **(A)**; (2.07 ± 0.57) × 10^8 M^{-1} s^{-1}, R^2 = 0.86 **(B)**.

References

S1. P. R. Zalupski, T. S. Grimes, C. R. Heathman and D. R. Peterman, *Appl. Spectrosc.*, 2017, **71**, 2608-2615.

S2. A. V. M. Gogolev, I. E.; Pikaev, A. K., presented in part at the Proc. Tihany Symp. Radiat. Chem., 1989.

S3. J. F. Wishart, A. R. Cook and J. R. Miller, *Rev. Sci. Instrum.*, 2004, **75**, 4359-4366.

S4. A. R. Cook, *J. Phys. Chem. A*, 2021, **125**, 10189-10197.

S5. A. R. Cook, M. J. Bird, S. Asaoka and J. R. Miller, *J. Phys. Chem. A*, 2013, **117**, 7712-7720.

S6. G. Garaix, G. P. Horne, L. Venault, P. Moisy, S. M. Pimblott, J. L. Marignier and M. Mostafavi, *J. Phys. Chem. B*, 2016, **120**, 5008-5014.

S7. J. H. Espenson, *Chemical Kinetics and Reaction Mechanisms*, McGraw-Hill, 1981.

S8. G. G. Manov, R. G. Bates, W. J. Hamer and S. F. Acree, *Journal of the American Chemical Society*, 2002, **65**, 1765-1767.

S9. A. M. P. Gogolev A.V.; Fedoseev, *High Energy Chem.*, 1988, **21**, 401-402.

S10. G. P. Horne, T. S. Grimes, P. R. Zalupski, D. S. Meeker, T. E. Albrecht-Schonzart, A. R. Cook and S. P. Mezyk, *Dalton Trans.*, 2021, **50**, 10853-10859.

S11. B. M. Rotermund, S. P. Mezyk, J. M. Sperling, N. B. Beck, H. Wineinger, A. R. Cook, T. E. Albrecht-Schonzart and G. P. Horne, *J Phys Chem A*, 2024, **128**, 590-598.

S12. G. P. Horne, B. M. Rotermund, T. S. Grimes, J. M. Sperling, D. S. Meeker, P. R. Zalupski, N. Beck, Z. K. Huffman, D. G. Martinez, A. Beshay, D. R. Peterman, B. H. Layne, J. Johnson, A. R. Cook, T. E. Albrecht-Schonzart and S. P. Mezyk, *Inorg. Chem.*, 2022, **61**, 10822-10832.

S13. A. J. Bard, R. Parsons and J. Jordan, *Standard Potentials in Aqueous Solution*, Marcel Dekker Inc., New York, 1985.